RAA 2018 Vol. **18** No. **2**, 21(12pp) doi: 10.1088/1674–4527/18/2/21

http://www.raa-journal.org *http://iopscience.iop.org/raa*

***R**esearch in*
***A**stronomy and*
***A**strophysics*

R-band host galaxy contamination of TeV γ-ray blazar Mrk 501: effects of aperture size and seeing

Hai-Cheng Feng[1,2,3], Hong-Tao Liu[1,3,4], Ying-He Zhao[1,3,4], Jin-Ming Bai[1,3,4], Fang Wang[5] and Xu-Liang Fan[6]

[1] Yunnan Observatories, Chinese Academy of Sciences, Kunming 650216, China; *htliu@ynao.ac.cn; zhaoyinghe@ynao.ac.cn*

[2] University of Chinese Academy of Sciences, Beijing 100049, China

[3] Key Laboratory for the Structure and Evolution of Celestial Objects, Chinese Academy of Sciences, Kunming 650216, China

[4] Center for Astronomical Mega-Science, Chinese Academy of Sciences, Beijing 100012, China

[5] School of Physics and Space Science, China West Normal University, Nanchong 637009, China

[6] School of Physics, Huazhong University of Science and Technology, Wuhan 430074, China

Received 2017 August 30; Accepted 2017 November 30

Abstract We simulated the R-band contribution of the host galaxy of TeV γ-ray BL Lac object Mrk 501 in different aperture sizes and seeing conditions. An intensive set of observations was acquired with the 1.02 m optical telescope, managed by Yunnan Observatories, from 2010 May 15 to 18. Based on the host subtraction data usually used in the literature, the subtraction of host galaxy contamination results in significant seeing-brightness correlations. These correlations would lead to illusive large amplitude variations at short timescales, which will mask the intrinsic microvariability, thus giving rise to difficulty in detecting the intrinsic microvariability. Both aperture size and seeing condition influence the flux measurements, but the aperture size impacts the result more significantly. Based on the parameters of an elliptical galaxy provided in the literature, we simulated the host contributions of Mrk 501 in different aperture sizes and seeing conditions. Our simulation data of the host galaxy obviously weaken these significant seeing-brightness correlations for the host-subtracted brightness of Mrk 501, and can help us discover the intrinsic short timescale microvariability. The pure nuclear flux is $\sim$8.0 mJy in the R band, i.e., the AGN has a magnitude of $R \sim 13.96$ mag.

Key words: galaxies: active — BL Lacertae objects: individual (Mrk 501) — techniques: photometric — methods: data analysis

1 INTRODUCTION

Blazars are an extreme subclass of active galactic nuclei (AGNs), including BL Lacertae (BL Lac) objects and flat spectrum radio quasars (FSRQs) (e.g., Angel & Stockman 1980; Urry & Padovani 1995; Fossati et al. 1998; Böttcher & Dermer 2002; Maraschi & Tavecchio 2003). They are characterized by rapid and strong variability over the whole electromagnetic spectrum, high and variable polarization from the optical to radio bands, and prominent non-thermal emission at all wavelengths. In general, these extreme properties can be generated from a relativistic jet with a viewing angle less than 10° (e.g., Blandford & Königl 1979; Urry & Padovani 1995). The broadband spectral energy distributions (SEDs) of blazars usually exhibit a double peak profile. The first component extends from infrared to ultraviolet or soft X-ray, and the second is located in the GeV/TeV gamma-ray bands (e.g., Ghisellini et al. 1998; Abdo et al. 2010). The first peak is generally believed to be the synchrotron radiation of relativistic electrons in the jet. The second peak is attributed to inverse-Compton scattering of the same electron population that produces the synchrotron radiation (e.g., Dermer & Schlickeiser 1993; Böttcher 2007; Neronov et al. 2012).

Due to the property of strong variability in BL Lac objects, the photometric technique is widely used to investigate the structures, radiation mechanisms, dynamics and masses of the central supermassive black holes (e.g., Ciprini et al. 2003, 2007; Gupta et al. 2008b; Liu & Bai 2015; Dai et al. 2015; Guo et al. 2017). However, the host galaxies often exhibit strong radiation in the optical to near-infrared (NIR) bands. Thus, contamination from the host galaxies may influence the photometric results, especially for nearby extended sources. The photometric aperture is either a dynamic aperture or a fixed aperture. A dynamic aperture could be a few times the seeing, and the case of an extended source will result in a significant dependence of the photometric magnitudes on the seeing. There is not a dependence on the seeing for a point source at high redshift. A fixed aperture and a dynamic aperture could result in similar influences on the photometric results for an extended source due to the seeing (see Feng et al. 2017). For point sources, strong host galaxies could dilute the variability amplitudes of AGNs. Besides, the color indices and the SEDs of AGNs will be influenced. Since an extended source is resolved, different aperture sizes and seeing conditions would introduce large uncertainties in photometry at different epochs.

However, the host galaxies of nearby BL Lac objects are elliptical galaxies, which are huge (with effective radius $R_{\rm e} \sim 10\,{\rm kpc}$) and luminous ($M_R \sim -24.0\,{\rm mag}$) (e.g., Falomo & Kotilainen 1999; Urry et al. 1999, 2000; Scarpa et al. 2000; Kotilainen & Falomo 2004; Nilsson et al. 2003, 2007; Hyvönen et al. 2007). Even though some BL Lac objects may show signs of interaction with companions (e.g., Stickel et al. 1993; Falomo 1996; Heidt et al. 1999; Falomo & Ulrich 2000), there is no clear evidence in most cases that the nuclear activity is triggered by interaction (Nilsson et al. 1999, 2007). For most BL Lac objects, the morphologies of host galaxies are indistinguishable from similar normal elliptical galaxies (Scarpa et al. 2000). Thus, the host galaxies of BL Lac objects can be simulated based on normal elliptical galaxies.

Mrk 501 is a prototype nearby BL Lac object (redshift $z = 0.034$), which has been widely studied over the past two decades in the entire electromagnetic spectrum (e.g., Stickel et al. 1993; Quinn et al. 1996; Catanese et al. 1997; Samuelson et al. 1998; Xie et al. 1999, 2001; Konopelko et al. 2003; Gupta et al. 2008a, 2012; Albert et al. 2007; Abdo et al. 2011; Shukla et al. 2015; Ahnen et al. 2017). In the high energy regime from X-ray to TeV, Mrk 501 is one of the brightest extragalactic sources (Abdo et al. 2011). Many studies attempted to investigate its properties in the optical bands (e.g., Xie et al. 1999, 2001; Gupta et al. 2008a, 2012; Xiong et al. 2016). Based on the host subtraction data presented in Nilsson et al. (2007), widely used in previous photometric studies, the subtraction of host galaxy contamination results in a significant seeing-magnitude correlation for Mrk 501 (Feng et al. 2017). Researches related to its variability will need a reasonable subtraction of the host galaxy, which should (partly) eliminate this significant seeing-brightness correlation.

In this paper, we present observations of Mrk 501 in the R band from 2010 May 15 to 18. In order to obtain the host components in different aperture radii and seeing conditions, we use a two-dimensional simulation method to model the host galaxy. The structure of this paper is as follows: Section 2 presents the observations and data reduction; Section 3 gives the details on simulations; Section 4 draws conclusions, and discussion is presented in Section 5.

2 OBSERVATIONS AND DATA REDUCTION

The observations of Mrk 501 were carried out with the 1.02 m optical telescope administered by Yunnan Observatories. This telescope is a classical Cassegrain telescope located in Kunming, China. An Andor AW436 CCD (2048×2048 pixels) camera was mounted at the f/13.3 Cassegrain focus of the 1.02 m telescope. The entire field of view of the CCD is $\sim 7.3 \times 7.3\,{\rm arcmin}^2$, and each pixel corresponds to $0.21''$ in both dimensions. The CCD readout noise and gain are 6.33 electrons and 2.0 electrons/ADU, respectively (e.g., Dai et al. 2015; Xiong et al. 2016). We selected the standard Johnson broadband filters to carry out observations in the R band, and 326 valid exposures were obtained in four nights from 2010 May 15 to 2010 May 18. The exposure time is 150 seconds for each frame. Table 1 presents the complete observation log. For each image, the standard stars are always in the same field as the object.

Because the magnitudes of the standard stars are considered constant, the brightness of the object could be calibrated using these standard stars (e.g., Bai et al. 1998; Fan et al. 2014; Zhang et al. 2004, 2008). There are six

Table 1 Observation Log and Results of IDV Observations of Mrk 501

Date (1)	N (2)	Exposure (s) (3)	σ (star 1 – star 6) (4)
2010 May 15	88	150	0.005
2010 May 16	88	150	0.007
2010 May 17	80	150	0.005
2010 May 18	70	150	0.005

Notes: Column (1): observation date; Col. (2): observation number; Col. (3): exposure time; Col. (4): standard deviation of the (star 1 – star 6).

standard stars, whose magnitudes have been measured in other works, in the field (Villata et al. 1998; Fiorucci & Tosti 1996). In order to improve the measurement accuracy of the object magnitude, the selection of standard stars should consider both the position in the field and the brightness. Star 1 is the brightest of all nearby standard stars (see fig. 9 in Villata et al. (1998) for numbering), and is very close to the object. Thus, we selected star 1 to calculate the object magnitude. However, there are some uncertainties, which may introduce some errors to the standard stars, i.e. the relative brightness of the standard stars may change in some images. So, another comparison star is necessary. Star 6 is the closest to the object, and is used as another standard star. We used the standard deviation of star 1 and star 6 (σ(star 1 – star 6)) to characterize the change. The standard deviation of the differential instrumental magnitude of star 1 – star 6 is $\sim$0.005 (see Table 1).

All of the observed data were reduced using the standard procedure in the Image Reduction and Analysis Facility (IRAF) software. For each night, we took the median of all the bias frames and generated a master bias. Then the master bias was subtracted from all the object image frames and flat-field image frames. We used the same method to generate the master flat-field, and then flat-field correction was performed. After the corrections of bias and flat-field were applied, aperture photometry was performed using the APPHOT task. Considering that the standard stars are point sources, an extraction aperture depending on full width at half maximum (FWHM), i.e., a dynamic aperture, was used to obtain the maximum signal-to-noise ratio (S/N) (Howell 1989). We found that the best S/N was obtained with the aperture radius of 1.2 FWHM (minimizing σ(star 1 – star 6)). For the target, we chose 19 fixed aperture radii from $1''$ to $10''$ to investigate properties of the host galaxy. The epoch, differential magnitude and FWHM of each image are listed in Tables 2–5.

Figure 1 shows the relationship between the FWHMs and magnitudes in different apertures for each night, and Figure 2 shows the corresponding relationship of the FWHMs and fluxes. Figures 1 and 2 indicate that both the FWHM and aperture affect the photometric results. The brightness increases as the aperture increases, and decreases as the seeing increases. An increasing aperture will collect more light, and increasing seeing will scatter more light out of the aperture.

3 SIMULATIONS OF HOST GALAXY

The host galaxy of Mrk 501 is an elliptical galaxy (e.g., Nilsson et al. 1999, 2003; Hyvönen et al. 2007). Thus, we simulated the host galaxy using a two-dimensional model, which assumes the surface brightness $I(r)$ follows the Sérsic law $\sim r^{\beta}$ (Sersic 1968; Caon et al. 1993; Nilsson et al. 1999). The formula for $I(r)$ is

$$I(r) = I(r_{\rm e}){\rm dex}\left\{-b_\beta\left[\left(\frac{r}{r_{\rm e}}\right)^{-\beta}-1\right]\right\}, \qquad (1)$$

where β is the shape parameter and $r_{\rm e}$ is the effective radius (containing half of the total luminosity). A β-dependent constant b_β is defined as

$$b_\beta = \frac{0.868}{\beta} - 0.142, \qquad (2)$$

and

$$I(r_{\rm e}) = \frac{f_{\rm R}}{K_\beta r_{\rm e}^2\,(1-\epsilon)}, \qquad (3)$$

where $f_{\rm R}$ is the total flux of the galaxy, ϵ is the ellipticity and K_β can be derived from

$$K_\beta = {\rm dex}\left(0.030\log^2\beta - 0.441\log\beta + 1.079\right), \qquad (4)$$

where dex means ${\rm dex}(x) = 10^x$. Equations (1) to (4) indicate that if we obtain the parameters of β, ϵ, $r_{\rm e}$ and $f_{\rm R}$, we could confirm the surface brightness ($I(r)$) distribution of the host galaxy. Combining with the position angle θ, we can simulate the host of Mrk 501 in the observed images. However, the lower resolution and relatively poor S/N restrict how accurately we can measure values of the above parameters. Fortunately, Nilsson et al. (1999) have obtained all the above parameters from high-resolution images in the R band. The free β + core model was adopted in our simulations (based on properties of BL Lac objects and the de Vaucouleurs model (e.g., Makino et al. 1990)). We simulated the host component of Mrk 501 and convolved the simulation results

Table 2 Data Observed on 2010 May 15

MJD	Apert													FWHM
(d)	1.0	1.5	2.0	2.5	3.0	3.5	4.0	4.5	5.0	5.5	6.0	6.5	...	10.0	(arcsec)
5331.699363	4.121	6.985	9.483	11.412	12.958	14.235	15.239	16.179	16.988	17.740	18.423	19.044	...	22.416	1.98
5331.701875	4.335	7.214	9.651	11.581	13.102	14.353	15.380	16.299	17.114	17.871	18.542	19.167	...	22.519	1.86
5331.703727	4.307	7.174	9.597	11.475	12.970	14.182	15.183	16.105	16.926	17.642	18.287	18.904	...	22.128	1.89
5331.705590	4.256	7.147	9.588	11.486	12.970	14.195	15.197	16.105	16.910	17.642	18.287	18.886	...	22.088	1.93
5331.707442	4.271	7.167	9.615	11.496	12.994	14.222	15.211	16.105	16.895	17.610	18.271	18.904	...	22.190	1.90
5331.711146	4.056	6.921	9.448	11.433	13.006	14.287	15.323	16.254	17.082	17.789	18.474	19.096	...	22.374	2.00
...	...	...	...	...	...	...	...	...	...	...	...	...	...	...	...
5331.692500	3.950	6.776	9.293	11.276	12.840	14.156	15.183	16.149	16.973	17.724	18.406	19.009	...	22.272	2.00

Notes: This table is available in its entirety in a machine-readable form in the online version of the journal at *http://www.raa-journal.org/docs/Supp/3443fengTable2.txt*. A portion is shown here for guidance regarding its form and content. MJD = JD – 2450000. Apert: aperture radius in units of arcsec, presented in Columns 2–15. The fluxes are in units of mJy.

Table 3 Data Observed on 2010 May 16

MJD	Apert													FWHM
(d)	1.0	1.5	2.0	2.5	3.0	3.5	4.0	4.5	5.0	5.5	6.0	6.5	...	10.0	(arcsec)
5332.644491	3.160	5.719	8.169	10.227	11.829	13.139	14.156	15.071	15.869	16.586	17.241	17.855	...	21.152	2.63
5332.647292	3.349	5.994	8.483	10.475	12.027	13.272	14.274	15.197	15.972	16.663	17.288	17.871	...	20.881	2.38
5332.649294	3.383	6.050	8.514	10.456	11.983	13.211	14.195	15.071	15.840	16.541	17.161	17.740	...	20.785	2.40
5332.651157	3.446	6.123	8.633	10.660	12.273	13.557	14.580	15.508	16.329	17.051	17.675	18.271	...	21.308	2.27
5332.653009	3.501	6.202	8.681	10.689	12.262	13.519	14.553	15.479	16.284	17.004	17.626	18.237	...	21.328	2.28
5332.654861	3.282	5.907	8.405	10.427	12.038	13.346	14.393	15.309	16.105	16.833	17.480	18.070	...	21.210	2.45
...	...	...	...	...	...	...	...	...	...	...	...	...	...	...	...
5332.829722	3.782	6.543	9.040	10.999	12.524	13.771	14.769	15.651	16.434	17.146	17.805	18.389	...	21.506	2.13

Notes: This table is available in its entirety at *http://www.raa-journal.org/docs/Supp/3443fengTable3.txt*. The other notes are the same as those in Table 2.

Table 4 Data Observed on 2010 May 17

MJD	Apert													FWHM
(d)	1.0	1.5	2.0	2.5	3.0	3.5	4.0	4.5	5.0	5.5	6.0	6.5	...	10.0	(arcsec)
5333.686539	4.079	6.921	9.370	11.245	12.734	13.924	14.906	15.782	16.571	17.256	17.888	18.474	...	21.565	2.01
5333.688796	4.053	6.902	9.327	11.183	12.617	13.771	14.728	15.565	16.329	17.004	17.610	18.187	...	21.289	2.05
5333.690648	3.803	6.591	9.081	11.009	12.524	13.745	14.742	15.637	16.419	17.114	17.773	18.338	...	21.486	2.19
5333.692500	3.931	6.745	9.174	11.050	12.501	13.695	14.634	15.494	16.254	16.926	17.529	18.086	...	21.074	2.13
5333.694352	3.761	6.543	9.006	10.898	12.341	13.532	14.486	15.337	16.090	16.755	17.352	17.904	...	20.843	2.18
5333.696215	4.193	7.069	9.492	11.338	12.757	13.911	14.837	15.680	16.419	17.082	17.707	18.271	...	21.250	1.98
...	...	...	...	...	...	...	...	...	...	...	...	...	...	...	...
5333.836632	3.645	6.382	8.883	10.928	12.547	13.860	14.947	15.898	16.755	17.529	18.203	18.834	...	22.128	2.17

Notes: This table is available in its entirety at *http://www.raa-journal.org/docs/Supp/3443fengTable4.txt*. The other notes are the same as those in Table 2.

Table 5 Data Observed on 2010 May 18

MJD	Apert													FWHM
(d)	1.0	1.5	2.0	2.5	3.0	3.5	4.0	4.5	5.0	5.5	6.0	6.5	...	10.0	(arcsec)
5334.700336	3.717	6.489	8.949	10.858	12.387	13.607	14.593	15.494	16.299	17.020	17.691	18.304	...	21.525	2.19
5334.702801	3.530	6.225	8.689	10.699	12.296	13.607	14.674	15.623	16.465	17.225	17.904	18.508	...	21.765	2.27
5334.704664	4.019	6.838	9.301	11.255	12.804	14.065	15.099	16.031	16.864	17.626	18.287	18.921	...	22.251	1.99
5334.706516	3.782	6.561	9.023	10.958	12.478	13.720	14.715	15.608	16.404	17.098	17.756	18.355	...	21.525	2.12
5334.708368	3.772	6.543	9.006	10.969	12.536	13.796	14.823	15.753	16.556	17.288	17.970	18.576	...	21.805	2.14
5334.710231	3.619	6.323	8.801	10.788	12.409	13.733	14.796	15.767	16.632	17.384	18.070	18.713	...	22.006	2.17
...	...	...	...	...	...	...	...	...	...	...	...	...	...	...	...
5334.833229	3.652	6.400	8.883	10.828	12.352	13.594	14.607	15.522	16.329	17.051	17.691	18.287	...	21.545	2.19

Notes: This table is available in its entirety at *http://www.raa-journal.org/docs/Supp/3443fengTable5.txt*. The other notes are the same as those in Table 2.

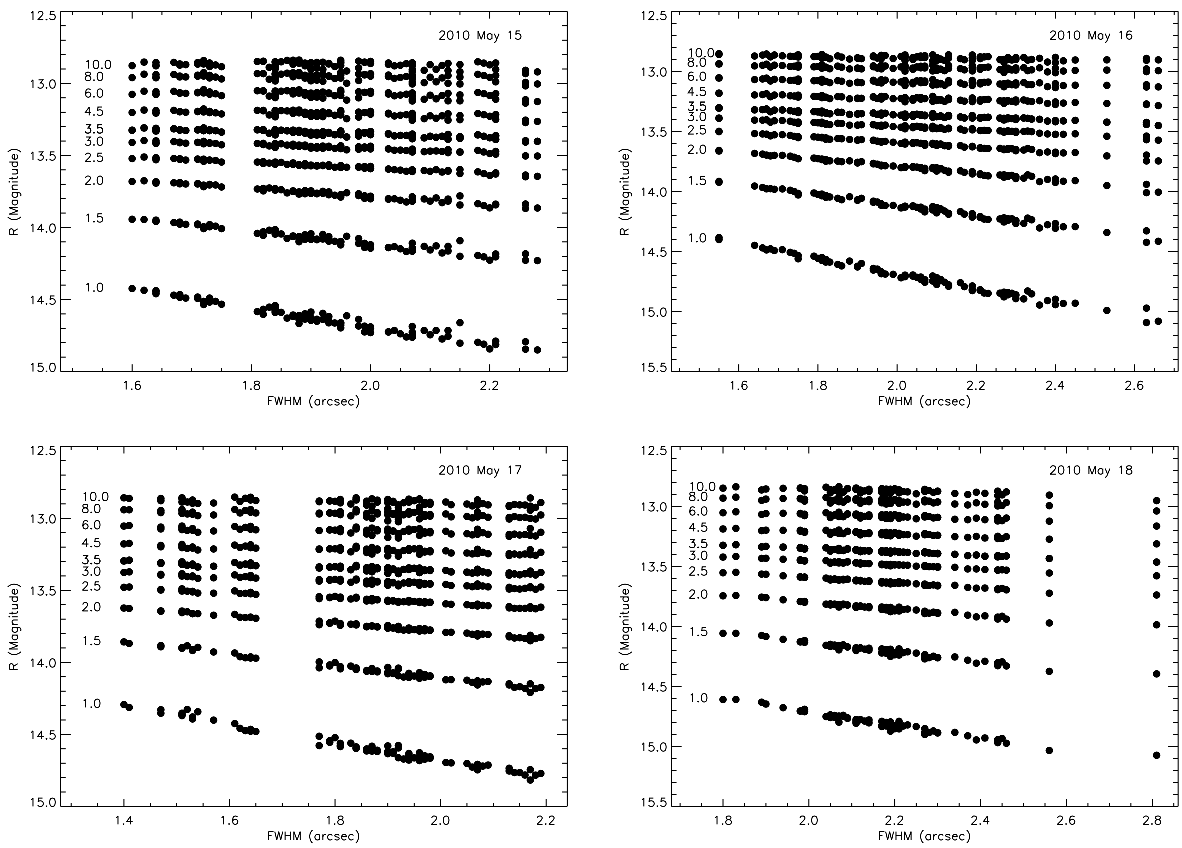

Fig. 1 The relationships between FWHM and magnitude for different photometric aperture radii in our observations.

into 28 different FWHMs with the point spread function (PSF) of a Gaussian profile. The FWHMs of the convolved images are from $0.5''$ to $5.9''$ with a bin size of $0.2''$. We performed the photometry using 111 fixed apertures from $1.0''$ to $12.0''$ with a bin size of $0.1''$. Table 6 shows flux simulations for the host galaxy under different FWHMs and apertures.

Figure 3 shows the relationships between brightness, FWHM and aperture. Our simulation results are very different from those in Nilsson et al. (2007). The host subtraction based on the subtraction data in Nilsson et al. (2007) led to a significant seeing-brightness correlation for Mrk 501 (see an example presented in fig. 2 in Feng et al. 2017). Thus, a reasonable host subtraction is needed for the optical photometry of Mrk 501.

We used two methods to compare the simulation results with our observations. First, we checked the observed images to determine photometric regions where the S/N ratios are high enough (i.e., > 5). This is normally achieved with an aperture radius of $5''$. We measured the brightness of the images within annular apertures with radii of $3.5'' - 4.5''$ and $4.5'' - 5.0''$.

Figure 4 shows comparisons between the simulated and observed results in the same annular apertures. The simulations and observations are (marginally) consistent with each other in the case of $3.5'' - 4.5''$ except for 2010 May 17 (see Fig. 4). In general, the observed results are less than the simulation results in the case of $4.5'' - 5.0''$. This may arise from low S/N ratios at those annular apertures. The host galaxy of Mrk 501 is a low surface brightness galaxy, and this will result in lower S/N ratios at larger annular apertures. The deviations of simulations from observations in the case of $3.5'' - 4.5''$ are less than those in the case of $4.5'' - 5.0''$. Combining four panels in Figure 4 into one panel (see Fig. 5), we find that simulations are marginally consistent with observations in the case of $3.5'' - 4.5''$, and the deviations of observations from simulations in the case of $3.5'' - 4.5''$ are less than those in the case of $4.5'' - 5.0''$. Observations need an exposure time to obtain a certain S/N ratio. A low S/N ratio may result in a lower flux measurement

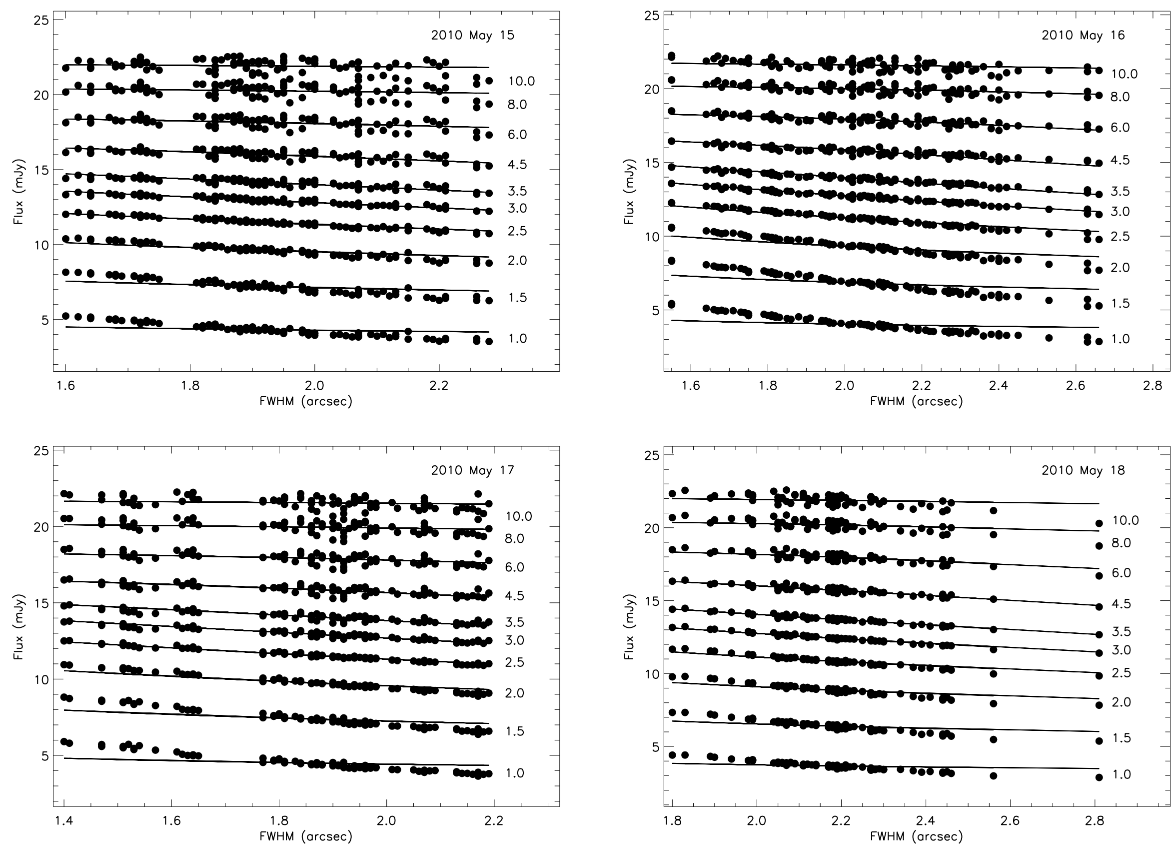

Fig. 2 The relationships between FWHM and flux for different photometric aperture radii in our observations. The solid lines are the simulation results moved vertically by the average differences between the original simulations and the corresponding observational data (the solid circles).

Table 6 Simulation Data for the Host Galaxy of Mrk 501

Apert	FWHM													
	0.5	0.7	0.9	1.1	1.3	1.5	1.7	1.9	2.1	2.3	2.5	2.7	2.9	...	5.9
1.0	2.615	2.138	1.732	1.425	1.190	1.012	0.872	0.762	0.672	0.599	0.537	0.486	0.441	...	0.164
1.1	2.928	2.456	2.023	1.681	1.413	1.207	1.043	0.913	0.806	0.719	0.646	0.585	0.532	...	0.199
1.2	3.231	2.775	2.322	1.949	1.649	1.415	1.226	1.076	0.951	0.850	0.764	0.692	0.630	...	0.236
1.3	3.512	3.082	2.620	2.222	1.893	1.632	1.419	1.249	1.106	0.990	0.891	0.808	0.736	...	0.277
1.4	3.782	3.383	2.920	2.503	2.147	1.860	1.623	1.431	1.271	1.139	1.026	0.931	0.849	...	0.321
1.5	4.034	3.668	3.213	2.783	2.405	2.095	1.834	1.622	1.443	1.296	1.168	1.062	0.969	...	0.368
...	...	...	...	...	...	...	...	...	...	...	...	...	...	...	...
12.0	15.554	15.542	15.527	15.509	15.486	15.460	15.429	15.394	15.354	15.311	15.259	15.206	15.143	...	12.889

Notes: This table is available in its entirety in a machine-readable form in the online version of the journal at *http://www.raa-journal.org/docs/Supp/3443fengTable6.txt*. A portion is shown here for guidance regarding its form and content. Apert: aperture radius in units of arcsec, presented in Col. (1). FWHM is in units of arcsec, presented in Cols. (2)–(16). The fluxes are in units of mJy.

compared to the flux simulation based on a high S/N ratio image presented in Nilsson et al. (1999). Another method is based on the fact that the brightness difference between simulation and observation is the contribution of AGN, i.e., the observed flux is a combination of AGN and its host galaxy flux, while the simulation result only contains the host component. For a relatively large photometric aperture (nearly including all the AGN flux, e.g., an aperture radius of $4.0''$ including 99% of the AGN flux), the differences between simulations and observations should be a constant for the different seeing conditions. The observed results are very consistent with the vertically shifted simulation results for aperture radii from $3.0''$ to $6.0''$ in the flux versus FWHM diagram (see

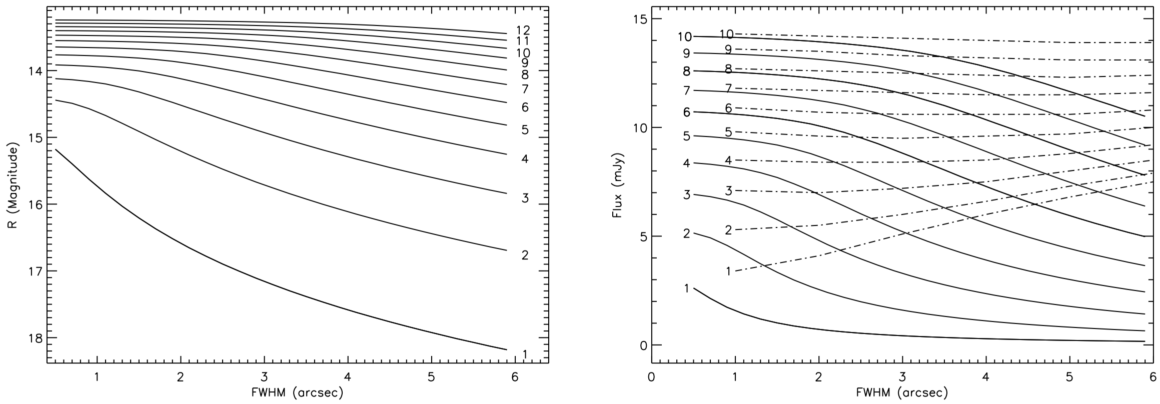

Fig. 3 The relationships between FWHM and brightness for different apertures with the simulated host galaxy of Mrk 501 (*solid lines*). The dot-dashed lines represent the results of Nilsson et al. (2007). The numbers associated with lines in the plots are the photometric aperture radii.

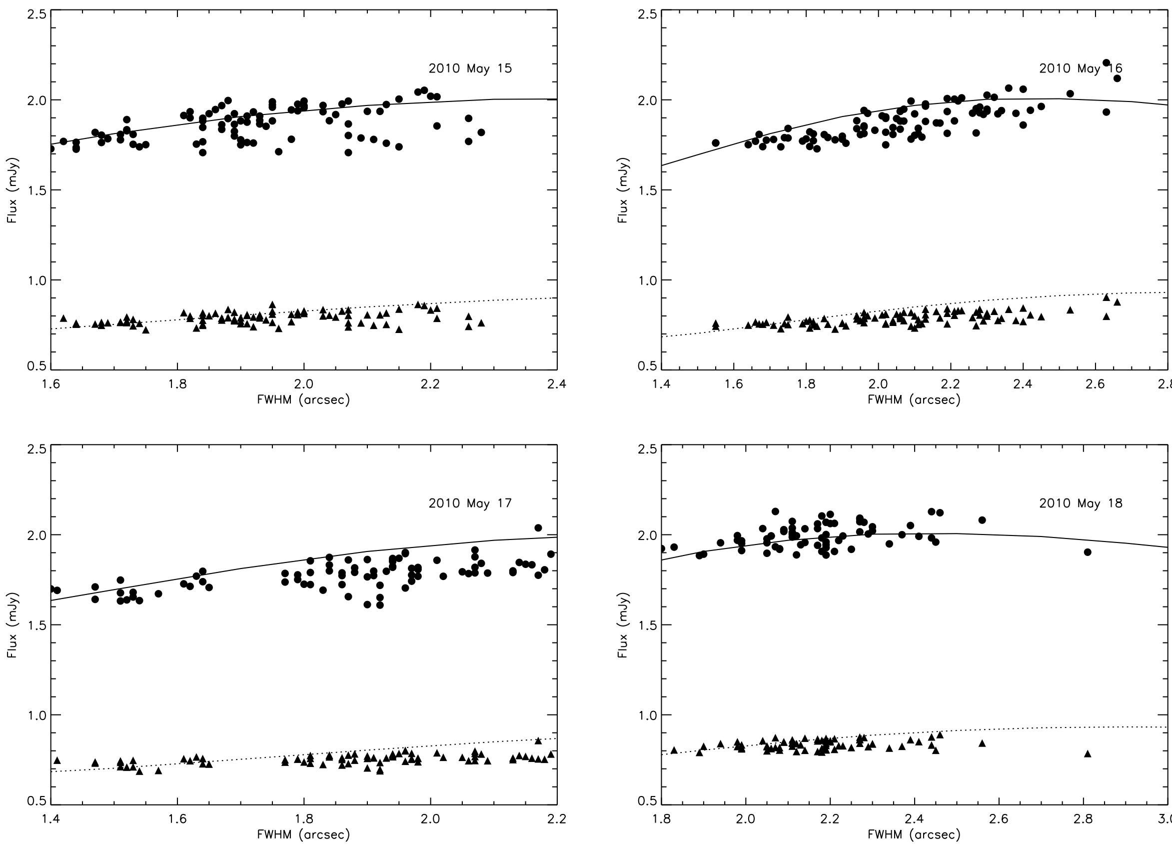

Fig. 4 Fluxes in annular apertures for different seeing (FWHM). In each panel, the solid line represents the simulation results from $3.5''$ to $4.5''$, and the circles represent the observed results in the same annular apertures. Also in each panel, the dotted line indicates the simulation results from $4.5''$ to $5.0''$, and the triangles indicate the observed results in the same annular apertures.

Fig. 2). There are very similar trends between the vertically shifted simulations and the observational results for the other aperture radii in Figure 2. These slight differences between simulations and observations may be from the fact that the corresponding aperture radii are either too small or too large ($< 3.0''$ or $> 6.0''$).

We calculated the average difference between the simulations and the observational results in Figure 2.

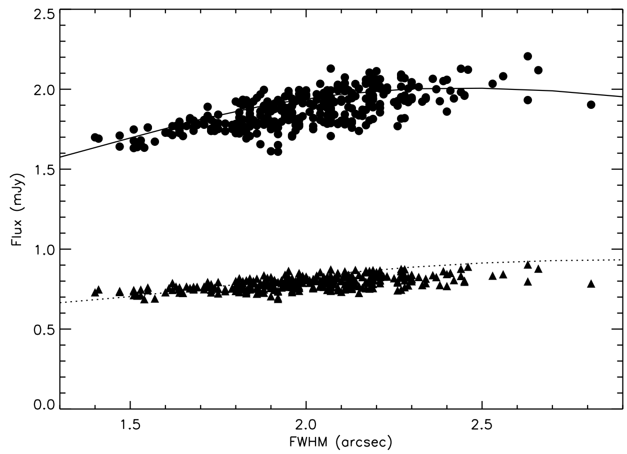

Fig. 5 Observational fluxes on 2010 May 15 – 18. The symbols are same as in Fig. 4.

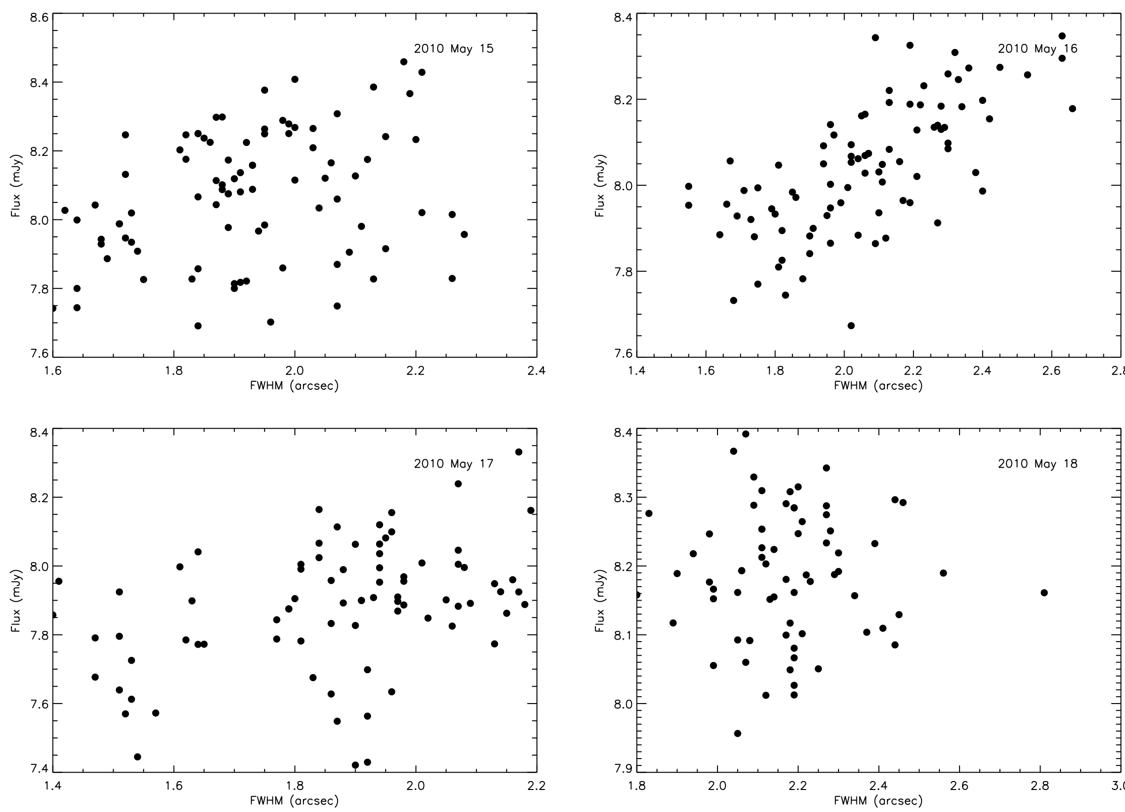

Fig. 6 AGN host-subtracted flux versus seeing (FWHM). The observed fluxes are measured for the photometric aperture radius of $4.0''$.

The shifted simulation results are very consistent with the observational data, and the average difference can be regarded as the AGN flux. The mean flux of the AGN is ∼8.0 mJy, which corresponds to $R = 13.96\,\mathrm{mag}$ ($F = 3.08\times10^{-0.4\times R+3}$ Jy (Nilsson et al. 2007)). Thus, the AGN's contribution to the total flux of the source is ∼13.3%. Compared with the brightness obtained in Nilsson et al. (1999), $R = 14.45\,\mathrm{mag}$, AGN Mrk 501 brightened by ∼57% in our observations. According to our simulations, we subtracted the host contribu-

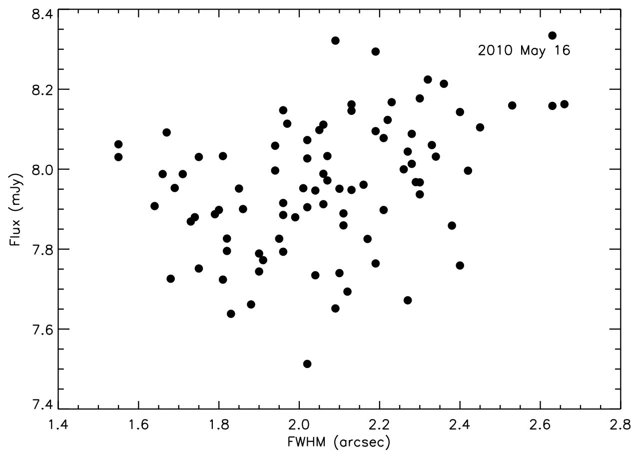

Fig. 7 AGN host-subtracted flux versus seeing (FWHM) on 2010 May 16 for an aperture radius of $5.0''$.

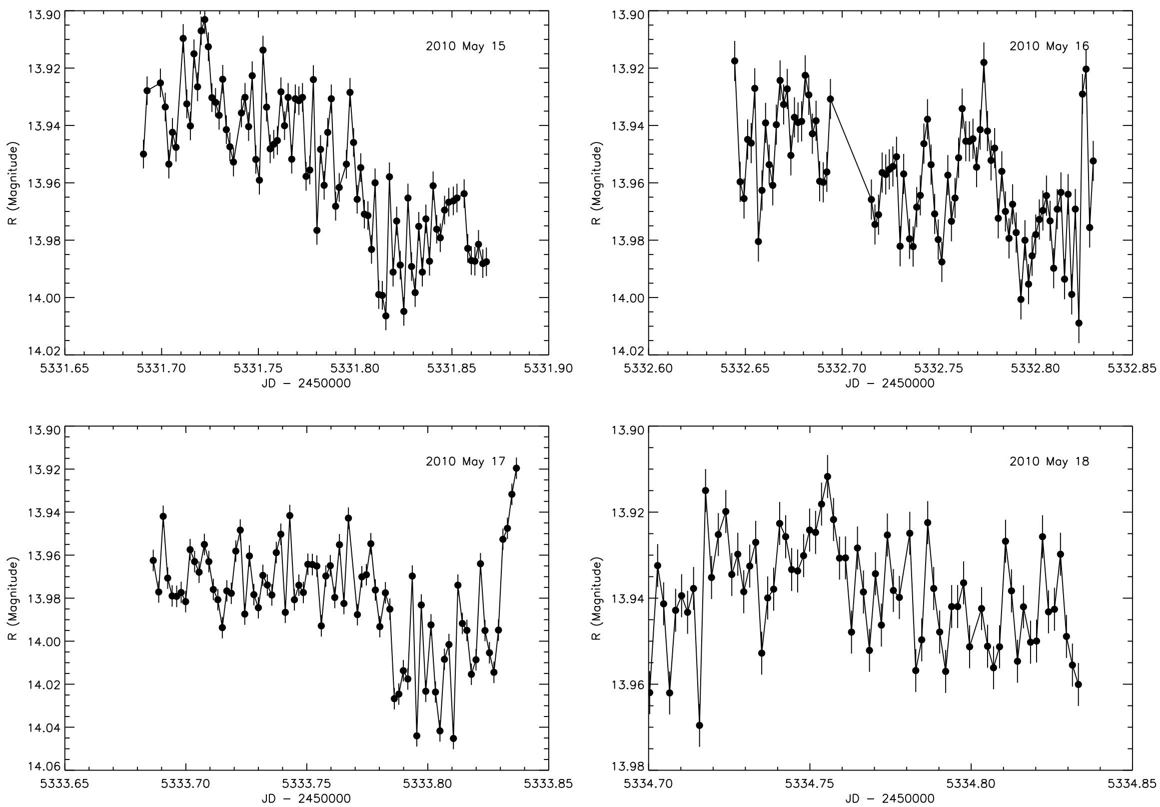

Fig. 8 AGN host-subtracted light curves for a photometric aperture radius of $4.0''$.

tion and investigated whether there are still significant seeing-brightness correlations for AGN Mrk 501. The host-subtracted fluxes versus FWHMs are presented in Figure 6. There is no correlation on 2010 May 18. Though the host-subtraction based on our simulations can (obviously) weaken the significant correlations found in Feng et al. (2017), there are still correlations for 2010 May 15 and 17, and an obvious correlation on 2010 May 16.

Figure 7 shows the host-subtracted flux versus seeing distribution in the case of a $5.0''$ aperture. The host-subtracted flux versus seeing distribution shows that the larger photometric aperture radii can further weaken the host-subtracted brightness-seeing correlation. Thus, our simulations can basically give a reasonable host-subtraction. The obvious correlation on 2010 May 16 might be from the smaller photometric aperture relative to the average seeing. The host-subtracted flux light curves show that the darkening variations found in Feng et al. (2017) still exist in the light curve on 2010 May 15 even though the host contribution has been subtracted (see Fig. 8). There is a flare with a duration of $\sim$1 hour on 2010 May 18 around MJD 5334.75 (see Fig. 8), which was not found in Feng et al. (2017). This confirms that the fake large amplitude fast variability due to the seeing effect can mask intrinsic microvariability in Mrk 501. This kind of fake rapid and strong variability due to the seeing effect will mask the intrinsic microvariability in Mrk 501, and will lead to difficulty in detecting intrinsic microvariability in similar sources with brighter host galaxies, e.g., Mrk 421.

4 CONCLUSIONS

Based on the intensive set of observations acquired with the 1.02 m optical telescope, administered by Yunnan Observatories, from 2010 May 15 to 18, and a two-dimensional model of an elliptical galaxy, we simulated the R-band contribution of the host galaxy of TeV γ-ray BL Lac object Mrk 501. The simulated brightness in the different aperture radii and seeing conditions shows correlations between the seeing and brightness for the host galaxy, and these correlations are confirmed well by the observational data. The differences between the simulation fluxes and the observational data are due to contribution from AGN Mrk 501, and the host-subtracted brightness of Mrk 501 can obviously weaken these significant correlations found in Feng et al. (2017). There is no correlation between the seeing and the host-subtracted brightness on 2010 May 18. However, there are correlations on 2010 May 15 and 17, and an obvious correlation on 2010 May 16. The larger photometric aperture radii with respect to the average seeing can further weaken the correlation on 2010 May 16 (see Figs. 6 and 2). These correlations led to illusive large amplitude variations on short timescales, which can mask the intrinsic microvariability and then lead to difficulty in detecting the intrinsic microvariability. The host-subtracted brightness light curves confirm the darkening variations on 2010 May 15 found in Feng et al. (2017), and revealed a flare with a duration of $\sim$1 hour on 2010 May 18. Both the aperture size and the seeing condition influence the photometric results, but the aperture size can have a stronger influence. The pure nuclear flux is $\sim$8.0 mJy. Compared with the result observed in July 1996 (Nilsson et al. 1999), the AGN Mrk 501 brightened by a factor of $\sim$57%. Simulation data of the host galaxy of Mrk 501 are given for the different aperture radii and seeing conditions (online Table 6).

5 DISCUSSION

The correlation between seeing FWHM and brightness within a certain aperture is obvious for the intensive set of observations acquired from 2010 May 15 to 18. At the same time, the flux of the target is higher as the aperture radius is larger. The larger aperture radius will cover more area of an extended source, and thus will collect more light in the aperture. Thus, the total brightness will be monotonically increasing with aperture radius. This indicates that a fixed aperture is better than a dynamic aperture in performing photometry for Mrk 501. This point was tested in Feng et al. (2017), where a fixed aperture was used to measure photometry. Brightness monotonically decreases with increasing FWHM of seeing in the fixed aperture. This can be explained in that the larger PSF due to the worse seeing will scatter more light out of a fixed aperture. Another feature is that the PSF effect is more significant for a smaller aperture (less than $3.0''$). This is due to the fact that the amount of scattered light from an AGN changes with different PSFs. Therefore, the photometry of Mrk 501 should use a large fixed aperture, which can collect almost all the light of an AGN. In addition, it is necessary to correct the influence of seeing.

Figure 3 shows the simulation results for the host galaxy of Mrk 501, and the two panels in Figure 3 have similar relationships as those in Figures 1 and 2. The brightness curve shapes from the simulation results are very similar to those of observations for the same aperture and the same range of FWHM. However, the results in Figure 3 are somewhat different from the results in Figures 1 and 2, especially for the small apertures, and this difference is mainly due to the AGN component. We tested the reliability of the simulations via two methods (see Sect. 3), and both tests indicate that the simulations are robust (see Fig. 2). The results in Figure 3 can be used to correct the host contamination of Mrk 501, and the corresponding values are given in Table 6. Nilsson et al. (2007) provided a similar table (table B.1). Comparing our simulation results to theirs (see Fig. 3), we found some differences. Though these two results indicate that the host fluxes strongly depend on photometric apertures, the values from the same aperture and PSF are inconsistent. Especially within a small aperture radius ($\leq 3.0''$), the difference is significant. For a fixed aperture, the relationships between brightness and FWHM are significantly different for these two results. The brightness of the host galaxy decreases as the FWHM increases (see Fig. 3). These trends are opposite to the results in Nilsson et al. (2007). The influence of the seeing on the variability amplitude is significant in our results. After we subtracted the contamination of the host galaxy using the results of Nilsson et al. (2007), the relationships are still significant for the brightness and seeing FWHM. Otherwise, if the brightness of the host galaxy monotonically increases with the FWHM, the outer part of the host galaxy would be brighter than the central part. This is inconsistent with the reversal of surface brightness distribution for an elliptical galaxy.

The simulations and observations indicate that the AGN contribution of Mrk 501 is $\sim$13.3%. This means that even if the variability of an AGN is up to 10%, we can only detect a magnitude change of $\sim 0.01\,\mathrm{mag}$ for the whole galaxy. This variability amplitude is approximately the limiting accuracy of photometry for some telescopes. Therefore, it is not easy to detect this variability in Mrk 501. The effects of the photometric aperture and observational seeing are significant for the photometric results, and most previous works did not take into account the effects of the two factors. This might lead to some fake variability in some previous works for Mrk 501, and the relevant results should be reconsidered. Our studies suggest that a fixed aperture, which depends on the seeing condition, is better than a dynamic aperture, and host galaxy subtraction is necessary. Our simulations give a reasonable host-subtraction. Strong host contamination also impacts the color, polarization and SED of an AGN. Thus, it is meaningful to subtract the host component before investigating properties of Mrk 501.

Acknowledgements We are grateful to the anonymous referee for constructive comments leading to significant improvement of this paper, and the editor for suggestions. We thank the financial supports of the Key Research Program of the CAS (Grant No. KJZD-EW-M06), the National Natural Science Foundation of China (NSFC; Grant No. 11433004) and the Ministry of Science and Technology of China (2016YFA0400700). We also thank the financial supports of the NSFC (Grant Nos. 11273052 and U1431228), and the Youth Innovation Promotion Association, CAS.

References

Abdo, A. A., Ackermann, M., Agudo, I., et al. 2010, ApJ, 716, 30

Abdo, A. A., Ackermann, M., Ajello, M., et al. 2011, ApJ, 727, 129

Ahnen, M. L., Ansoldi, S., Antonelli, L. A., et al. 2017, A&A, 603, A31

Albert, J., Aliu, E., Anderhub, H., et al. 2007, ApJ, 669, 862

Angel, J. R. P., & Stockman, H. S. 1980, ARA&A, 18, 321

Bai, J. M., Xie, G. Z., Li, K. H., Zhang, X., & Liu, W. W. 1998, A&AS, 132, 83

Blandford, R. D., & Königl, A. 1979, ApJ, 232, 34

Böttcher, M., & Dermer, C. D. 2002, ApJ, 564, 86

Böttcher, M. 2007, Ap&SS, 309, 95

Caon, N., Capaccioli, M., & D'Onofrio, M. 1993, MNRAS, 265, 1013

Catanese, M., Bradbury, S. M., Breslin, A. C., et al. 1997, ApJ, 487, L143

Ciprini, S., Tosti, G., Raiteri, C. M., et al. 2003, A&A, 400, 487

Ciprini, S., Takalo, L. O., Tosti, G., et al. 2007, A&A, 467, 465

Dai, B.-Z., Zeng, W., Jiang, Z.-J., et al. 2015, ApJS, 218, 18

Dermer, C. D., & Schlickeiser, R. 1993, ApJ, 416, 458

Falomo, R. 1996, MNRAS, 283, 241

Falomo, R., & Kotilainen, J. K. 1999, A&A, 352, 85

Falomo, R., & Ulrich, M.-H. 2000, A&A, 357, 91

Fan, J. H., Kurtanidze, O., Liu, Y., et al. 2014, ApJS, 213, 26

Feng, H.-C., Liu, H. T., Fan, X. L., et al. 2017, ApJ, 849, 161

Fiorucci, M., & Tosti, G. 1996, A&AS, 116, 403

Fossati, G., Maraschi, L., Celotti, A., Comastri, A., & Ghisellini, G. 1998, MNRAS, 299, 433

Ghisellini, G., Celotti, A., Fossati, G., Maraschi, L., & Comastri, A. 1998, MNRAS, 301, 451

Guo, Q., Xiong, D. R., Bai, J. M., Fan, X. L., & Yi, W. M. 2017, RAA (Research in Astronomy and Astrophysics), 17, 82

Gupta, A. C., Deng, W. G., Joshi, U. C., Bai, J. M., & Lee, M. G. 2008a, New Astron., 13, 375

Gupta, A. C., Fan, J. H., Bai, J. M., & Wagner, S. J. 2008b, AJ, 135, 1384

Gupta, S. P., Pandey, U. S., Singh, K., et al. 2012, New Astron., 17, 8

Heidt, J., Nilsson, K., Sillanpää, A., Takalo, L. O., & Pursimo, T. 1999, A&A, 341, 683

Howell, S. B. 1989, PASP, 101, 616

Hyvönen, T., Kotilainen, J. K., Falomo, R., Örndahl, E., & Pursimo, T. 2007, A&A, 476, 723

Konopelko, A., Mastichiadis, A., Kirk, J., de Jager, O. C., & Stecker, F. W. 2003, ApJ, 597, 851

Kotilainen, J. K., & Falomo, R. 2004, A&A, 424, 107
Liu, H. T., & Bai, J. M. 2015, AJ, 149, 191
Makino, J., Akiyama, K., & Sugimoto, D. 1990, PASJ, 42, 205
Maraschi, L., & Tavecchio, F. 2003, ApJ, 593, 667
Neronov, A., Semikoz, D., & Taylor, A. M. 2012, A&A, 541, A31
Nilsson, K., Pursimo, T., Takalo, L. O., et al. 1999, PASP, 111, 1223
Nilsson, K., Pursimo, T., Heidt, J., et al. 2003, A&A, 400, 95
Nilsson, K., Pasanen, M., Takalo, L. O., et al. 2007, A&A, 475, 199
Quinn, J., Akerlof, C. W., Biller, S., et al. 1996, ApJ, 456, L83
Samuelson, F. W., Biller, S. D., Bond, I. H., et al. 1998, ApJ, 501, L17
Scarpa, R., Urry, C. M., Padovani, P., Calzetti, D., & O'Dowd, M. 2000, ApJ, 544, 258
Sersic, J. L. 1968, Atlas de Galaxias Australes (Cordoba, Argentina: Observatorio Astronomico)
Shukla, A., Chitnis, V. R., Singh, B. B., et al. 2015, ApJ, 798, 2
Stickel, M., Fried, J. W., & Kuehr, H. 1993, A&AS, 98, 393
Urry, C. M., & Padovani, P. 1995, PASP, 107, 803
Urry, C. M., Falomo, R., Scarpa, R., et al. 1999, ApJ, 512, 88
Urry, C. M., Scarpa, R., O'Dowd, M., et al. 2000, ApJ, 532, 816
Villata, M., Raiteri, C. M., Lanteri, L., Sobrito, G., & Cavallone, M. 1998, A&AS, 130, 305
Xie, G. Z., Li, K. H., Zhang, X., Bai, J. M., & Liu, W. W. 1999, ApJ, 522, 846
Xie, G. Z., Li, K. H., Bai, J. M., et al. 2001, ApJ, 548, 200
Xiong, D., Zhang, H., Zhang, X., et al. 2016, ApJS, 222, 24
Zhang, X., Zhang, L., Zhao, G., et al. 2004, AJ, 128, 1929
Zhang, X., Zheng, Y. G., Zhang, H. J., & Hu, S. M. 2008, ApJS, 174, 111